AIAA 2003-3890

Unsteady Computations of a Jet in Crossflow with Ground Effect
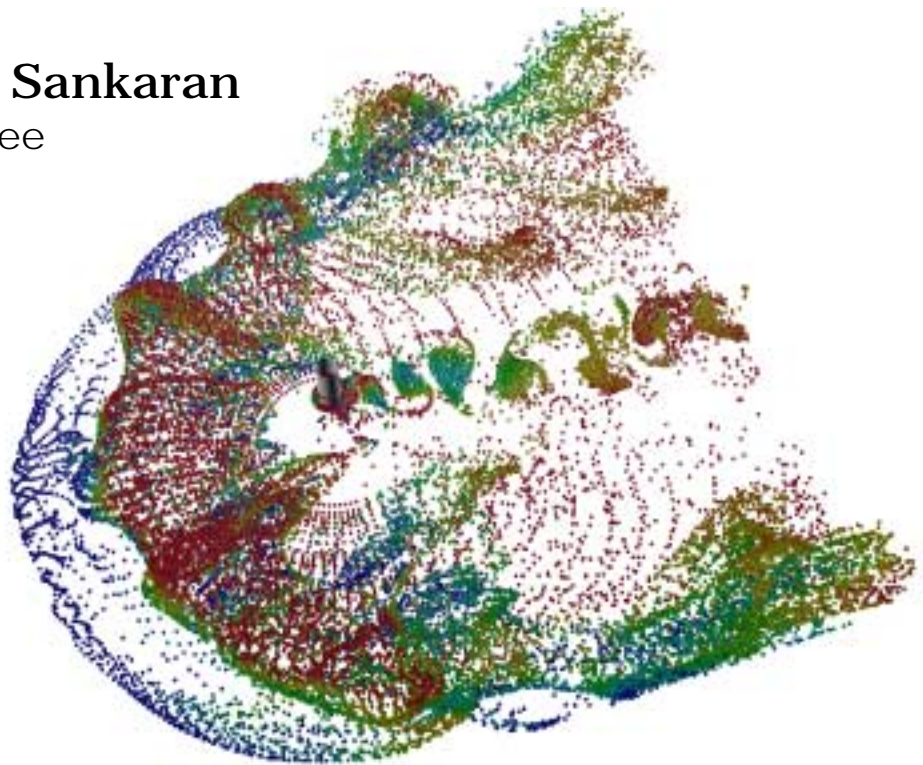
Shishir A. Pandya
NASA Ames Research Center
Moffett Field, CA

Scott M. Murman
ELORET
Moffett Field, CA

Venkateswaran Sankaran
University of Tennessee
Tullahoma, TN

33rd AIAA Fluid Dynamics Conference and Exhibit
23-26 June 2003 / Orlando, FL

AIAA 2003-3890

Unsteady Computations of a Jet in Crossflow with Ground Effect

Shishir A. Pandya [*]
NASA Ames Research Center
Moffett Field, CA

Scott M. Murman [†]
ELORET
Moffett Field, CA

Venkateswaran Sankaran [‡]
University of Tennessee
Tullahoma, TN

Abstract

A jet impinging on the ground plane in a low-speed crossflow is studied computationally using the OVERFLOW code with an unsteady low-Mach number preconditioner. The results are compared to experimental data to verify that the gross features of the flow can be accurately simulated with reasonable efficiency on a computer. The unsteadiness of the ground vortex is the focus of the investigation with intent of predicting the cycle of vortex formation, growth and collapse.

Introduction

The study of a jet impinging on a ground in crossflow has been the subject of both experimental[1–4] and numerical[5, 6] studies. Of interest is jet powered V/STOL vehicle behavior in near-hover conditions such as an F-35B(See Fig. 1) during a vertical landing maneuver. During a landing, the jets of the vehicle are pointed toward the ground and due to the interaction of the jet with the ground, a ground vortex is created. Issues such as the extent, location, strength, and frequency of the ground vortex are crucial for the safety of the ground crew and for assessing hot gas ingestion effects on aircraft engine operation.

Fig. 1 F-35B(JSF) aircraft in hover. Two jets, one from the rear nozzle and one from a lift fan in front of the compressor provide powered lift. Image courtesy of Lockheed-Martin.

When the jet impinges on the ground, the air flows radially outward from the point of impact. A ground vortex is created in the shape of a horseshoe due to the presence of low speed cross flow (See Fig. 2). Experimental studies of the jet with and without crossflow were performed by Colin and Olivari[1]. These demonstrated the ground vortex and made observations about the location of the vortex separation point, however, no unsteady behavior is reported. Later experiments by Cimbala et al. [2, 3] describe an unsteady ground vortex behavior where the vortex forms, bursts and forms again. Frequency and vortex

---
[*]Aerospace Engineer, Member AIAA
[†]Senior Research Scientist, Member AIAA
[‡]Research Professor, Member AIAA

location observations are reported and are used for comparison in this paper. A more recent set of experiments by Barata[4, 7, 8] focuses on the turbulent aspects of the flow field.

Numerical studies of a jet in cross flow[5] and V/STOL aircraft[6, 9, 10] have also been successfully performed. In the numerical investigation of Ref. [5], the flow did not exhibit unsteady behavior. In the studies of Refs. [6, 9, 10], an entire Harrier aircraft is simulated with the complex multi-jet flow field. However, experimental verification of the ground vortex prediction is not available. In the current paper, the focus is on unsteady simulations of a single round jet in cross flow with ground effect for comparison with the experiments of Cimbala et al. [3].

The unsteady jet computations are obtained using the OVERFLOW code[11]. A preconditioned dual-time scheme[12] is used in order to obtain accurate results for the low speed crossflow with reasonable efficiency. Results shown in this paper demonstrate that the gross features of the flow field are well represented and the unsteady features associated with the ground vortex agrees with the experiment.

The problem configuration of the Cimbala et al. experiment[3] is discussed followed by a summary discussion of the numerical technique. A solution which represents the gross features of the flow field is then presented along with results which mimic a smokewire to show time-dependent behavior. The physical modeling aspect of the computation is discussed next followed by a parametric study varying the crossflow velocity.

Problem Configuration

The present simulation is designed to match the conditions in the experiment of Ref. [3]. The experiment was conducted in a test section where the top wall is 21 inches above the bottom wall. A circular tube is inserted through the top wall and is 16.5 inches in length leaving a 4.5 inch gap where the free jet develops before it hits the ground. The tube exit is 1.5 inches in diameter. The walls of the wind tunnel are 48 inches apart with the tube mounted at the center of the test section. The problem configuration is shown in Fig. 2.

The air exits the tube at a speed of 150 ft/s or Mach 0.13. The speed of the air flow in the wind
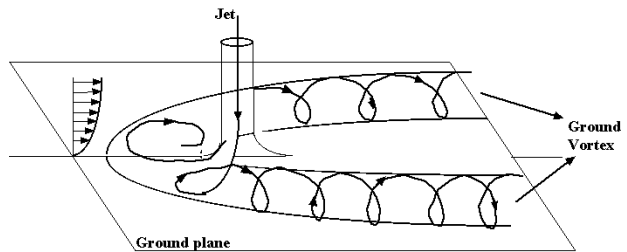

Fig. 2   Jet in crossflow.

tunnel is 15 ft/s (Mach number of 0.013) and is referred to as crossflow. The Reynolds number based on the crossflow speed and jet diameter is 80000.

The flow field associated with the present test case has flow features at several different scales. The air flows out of the circular tube into the test section generating lip vortices with a shedding frequency of approximately 100Hz. A second set of shed vortices created by the crossflow interaction with the cylindrical jet tube. The typical frequency associated with this von Kármán vortex street is approximately 10Hz.

Finally, when the jet impinges on the ground, the air flows radially outward from the point of impact. When this radially splaying flow meets the crossflow, the result is a ground vortex in the shape of a horseshoe around the free jet. The ground vortex is fed by the jet continually and begins to grow. This growth can not be sustained by the flow field and eventually results in a chaotic collapse of the the ground vortex. This "puffing" behavior is observed to occur at frequencies of O(1Hz)[3].

Computational Model
Equations of Motion

The OVERFLOW[11] Navier-Stokes flow solver is used to perform the present computations. The preconditioned dual-time stepping method in OVERFLOW is based on the dual-time-stepping methods presented in references[13, 14]. The Navier-Stokes equations can be written in conservative form as

$$\Gamma_p \frac{\partial Q}{\partial \tau} + \frac{\partial Q}{\partial t} + \frac{\partial E}{\partial x} + \frac{\partial F}{\partial y} + \frac{\partial G}{\partial z} = L(Q) \quad (1)$$

where $Q = [\rho, \rho u, \rho v, \rho w, e]^T$ is the vector of unknowns, E, F, and G are the inviscid fluxes and $L(Q)$ represents the viscous terms. Γ_p is the preconditioning matrix. The artificial time term $\frac{\partial Q}{\partial \tau}$

American Institute of Aeronautics and Astronautics

is introduced to the governing equations in order to provide a relaxation (sub-iteration) procedure between physical time steps. Termed dual-time-stepping, the sub-iteration process is important for ensuring efficient convergence of the time-dependent solutions at each physical time step. In combination with preconditioning, it also allows the use of larger time steps to efficiently capture the low frequency puffing of the ground vortex. The preconditioning formulation is also important for insuring accuracy at the low Mach number conditions of the crossflow. In generalized coordinates, the Navier-Stokes equations are discretized with first-order-accurate, Euler-implicit discretization for the artificial time term, second-order-backward difference discretization for the physical time terms and central-difference discretization for the spatial terms to obtain

$$I + \Delta\tau\Gamma_e S_p^{-1} A^k \delta\xi + \Delta\tau\Gamma_e S_p^{-1} B^k \delta\eta \qquad (2)$$
$$+ \Delta\tau\Gamma_e S_p^{-1} C^k \delta\zeta = \Gamma_e S_p^{-1} R^k$$

where $Q = J^{-1}Q$, $S_p = \Gamma_p + \frac{3}{2}\frac{\Delta\tau}{\Delta t}\Gamma_e$, $\Gamma_e = \frac{\partial Q}{\partial Q_p}$ (a transformation matrix between conservative and primitive variables), A, B, and C are the flux Jacobians and

$$R^k = -\Delta\tau\left(\frac{3\hat{Q}^k - 4\hat{Q}^n + \hat{Q}^{n-1}}{2\Delta t}\right) \qquad (3)$$
$$-\Delta\tau(\delta_\xi \hat{E}^k + \delta_\eta \hat{F}^k + \delta_\zeta \hat{G}^k)$$

The variable n is the time step counter while the variable k is the sub-iteration counter. Finally, $\Delta Q = Q^{k+1} - Q^k$. A diagonalized approximate factorization algorithm[15] is used for the solution of this equation. When converged in artificial time, this method is formally second-order accurate in time.

Code Description

The dual-time preconditioned algorithm in OVERFLOW is well-suited for treating multi-scale problems. The problem of a jet in low-speed crossflow has the low-speed oncoming flow which can be treated with an incompressible method and a jet which can be modeled with a compressible technique. To capture both scales in the same problem accurately, the low-Mach number preconditioner for the compressible formulation of OVERFLOW combined with the dual-time stepping algorithm is robust, efficient, and accurate. This algorithm allows the user to choose the time step appropriate for the problem being solved. In the current work, the time step was chosen to resolve the low-frequency puffing of the ground vortex. The ability to efficiently use a larger time step leads to a savings of one order of magnitude in CPU time over a non-preconditioned scheme for the current problem.

A low Mach number preconditioner based on Refs. [14] is used to capture the $M_\infty = 0.013$ crossflow accurately. Not using the low-Mach preconditioner leads to excessive damping at these conditions[12]. To ensure accuracy, 100 sub-iterations per time step are performed for an average sub-iteration convergence of 2 orders of magnitude. A time step is chosen based on the need to capture flow features on the order of 1Hz with approximately 100 time steps. The implementation of a low Mach number preconditioner for unsteady flows in OVERFLOW is discussed in detail in Ref. [12].

Grid System

Unlike a full aircraft simulation, the single jet has the advantage that there is no complex geometry involved. Thus, the choice of the mesh is driven more by the need to capture the ground vortex accurately. The overset, structured grid approach[16, 17] is used with 14 overlapping meshes. A representative view of these meshes is shown in Fig. 3.

The 14 structured meshes resolve either a geometrical or a flow feature. The geometric features of interest are the wind tunnel walls, and the jet tube. A cylindrical tube is placed at the center of the mesh system and is defined by two meshes. One mesh defines the walls and lip of the tube, while the other mesh covers the region inside the tube. A collar grid connects the tube to the top wall. Each wall of the wind tunnel is specified with an individual mesh. For the first cell next to the ground $y^+ \leq 1$ where the boundary layer remains attached. In the jet impingement region, $y^+ \leq 2$ in the first cell.

The flow features of interest are the jet impingement on the ground plane and the ground vortex. In order to provide adequate mesh resolution to capture these flow features, a mesh with
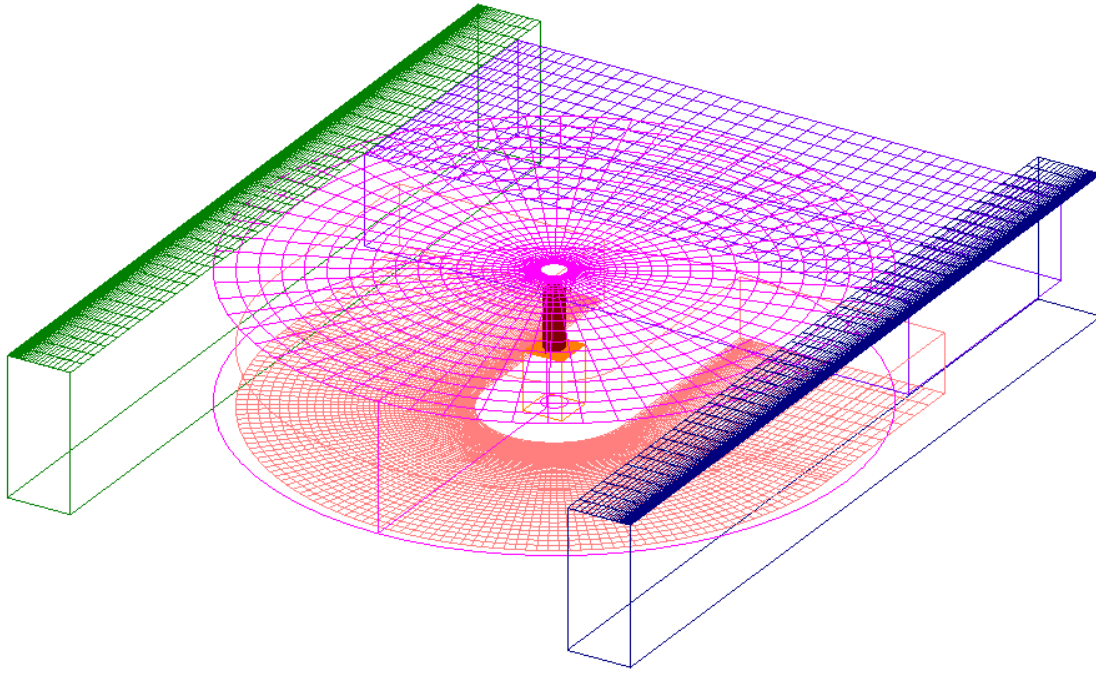
Fig. 3 A part of the grid system. Side wall grids, top wall grid(cylindrical), vortex grid, jet grid and lip grid are shown.

fine spacing is created for these regions. Due to the flexibility of the overset grid system, most of the 1.67 million points in the mesh are used to capture either a boundary layer or the important features of the flow.

Representative Solution

To illustrate the applicability of the dual-time preconditioned method on the problem of interest, the jet velocity is set to 150 ft/s (Mach 0.13) in a crossflow velocity of 15 ft/s (Mach 0.013). An overview of the flow field in Fig. 4 shows the ground vortex is upstream (to the left) of the jet and has a highly complex three-dimensional structure. The trailing von Kármán vortex street can also be seen downstream of the jet tube. This von Kármán vortex street has an approximate frequency of 25Hz ($St \approx 0.2$).

A cutting plane upstream of the jet in Fig. 5 shows the velocity vectors. A ground vortex with height approximately equal to the jet diameter is also present. This compares well with the mean velocity plotted in Fig. 4 of Ref. [3]. The boundary layer on the bottom wind tunnel wall can also be seen in this figure.

A plot mimicing oil flow on the surface and on the cutting plane along the centerline is shown in Fig. 6. The ground plane reveals the horse-shoe structure of the separation. In addition, the oil patterns on the ground also reveal that there are two separation lines with a reattachment line between them. The oil flow in the cutting plane captures the topology of the flow in the region of the ground vortex and is depicted in Fig. 7. The cutting plane shows two small, counter-rotating vortices in front of the large ground vortex. A separation line (S2 in Fig. 7) divides the secondary vortex from the ground vortex. Another vortex is present near the oncoming flow separation (S1). This vortex and the secondary vortex are divided by a reattachment line (A). These two counter-rotating vortices are also separated from the flow field above by a saddle point which receives flow from upstream and downstream and releases flow up and down. Most of the oncoming flow bypasses this entire structure of vortices and passes over the top of the ground vortex. While this behavior is characteristic of the flow field when the ground vortex is dominant, in general the unsteadiness of the ground vortex and the puffing behavior are resposible for the repeated creation and collapse of these features.

In order to ascertain if our results match the unsteady behavior reported by Cimbala et al. [3], we mimic the experimental measurements with a
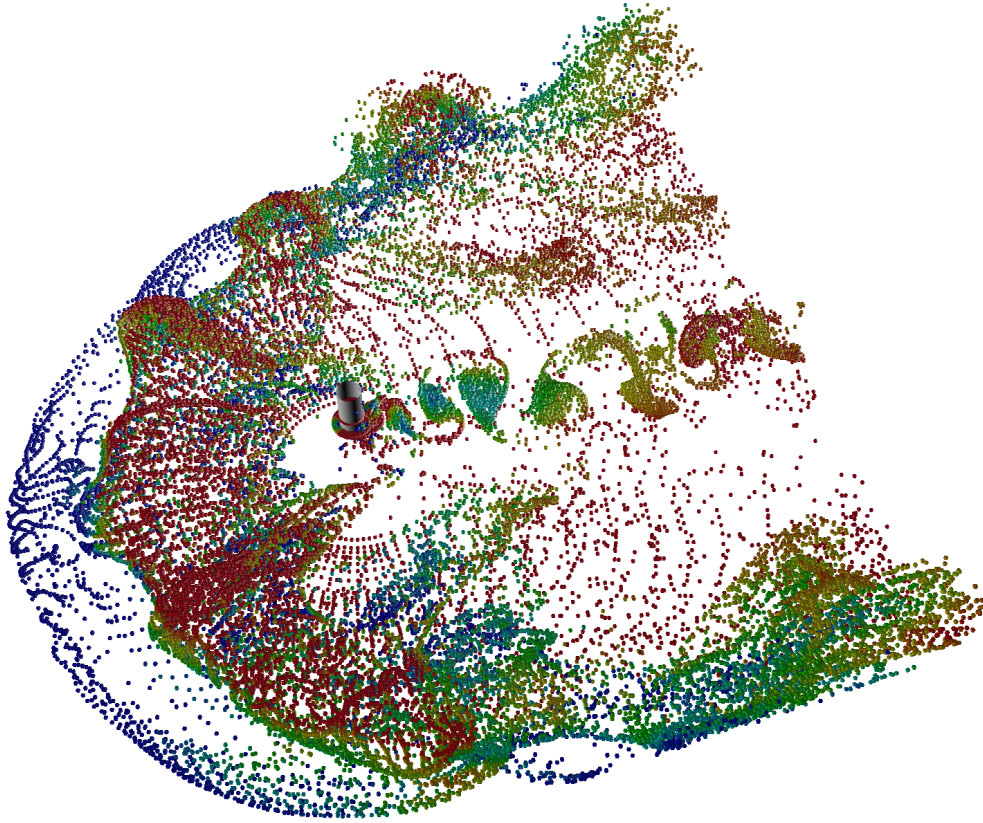
Fig. 4   Overview of the flow field for $M_\infty = 0.013$, $M_{jet} = 0.13$. **A ground vortex forms upstream of the jet with a von Kármán vortex street behind the jet tube.**
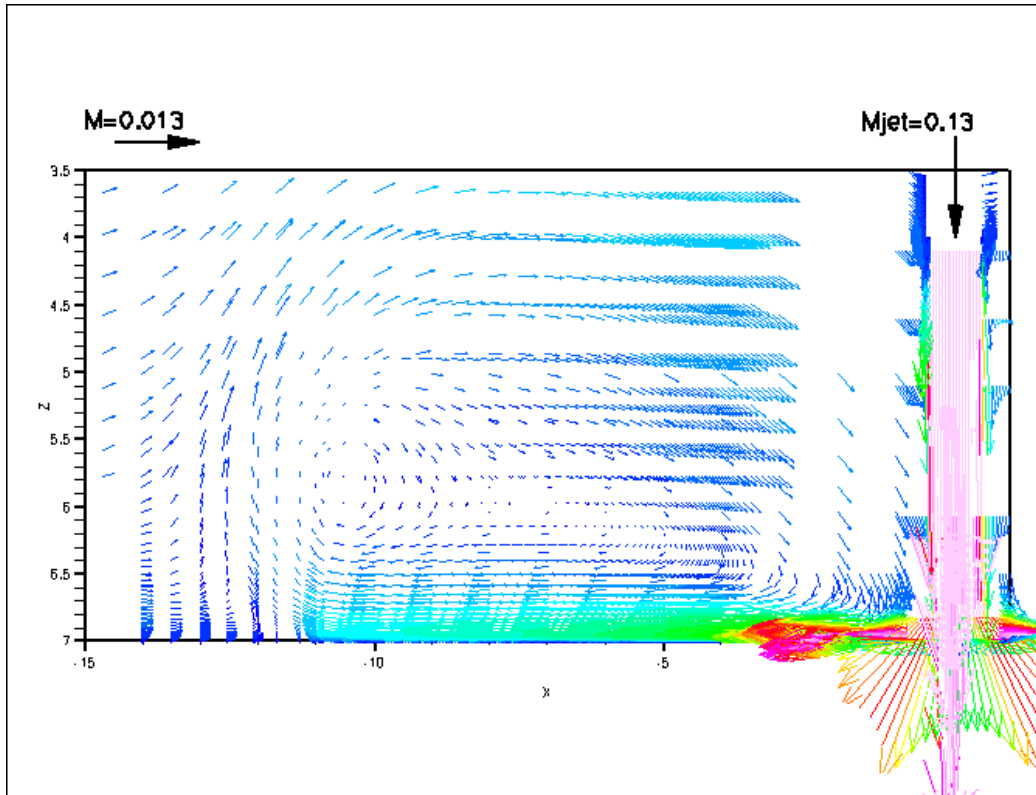

Fig. 5   Mean velocity vectors in the ground vortex region for $M_\infty = 0.013$, $M_{jet} = 0.13$.
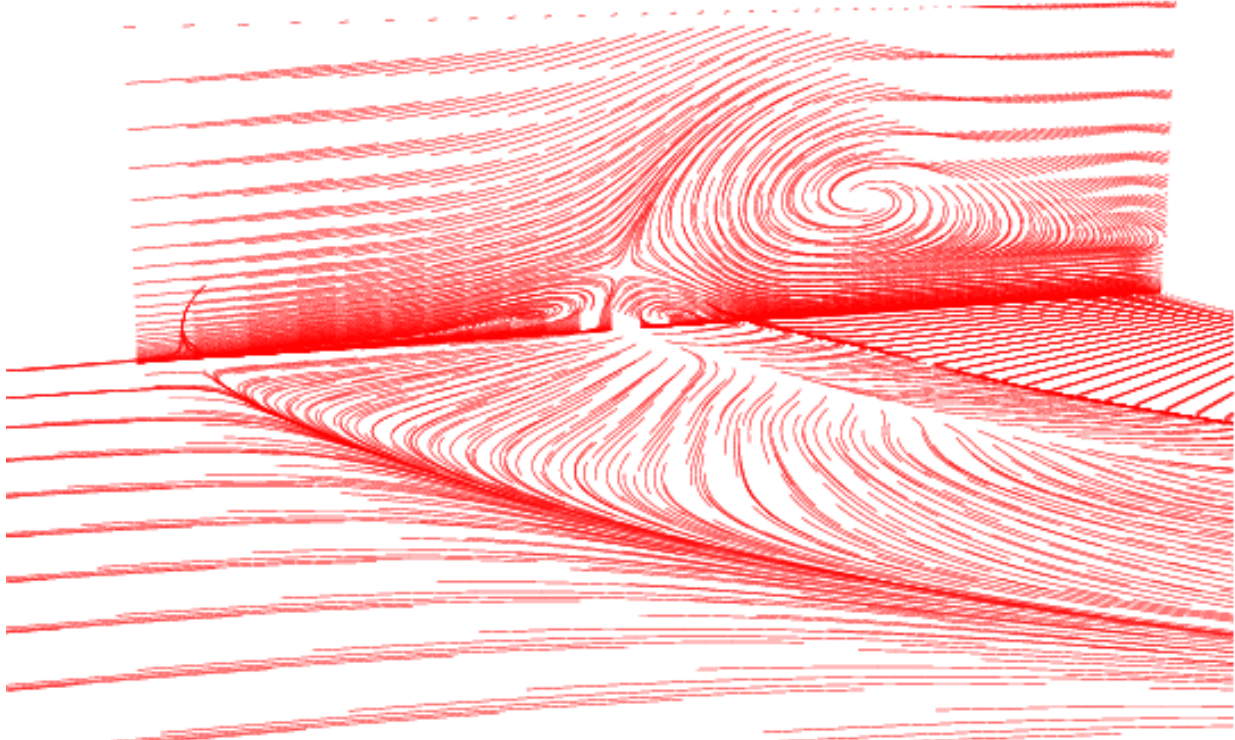
American Institute of Aeronautics and Astronautics

Fig. 6   Typical oil flow on the ground plane and in a cutting plane through the center of the domain.
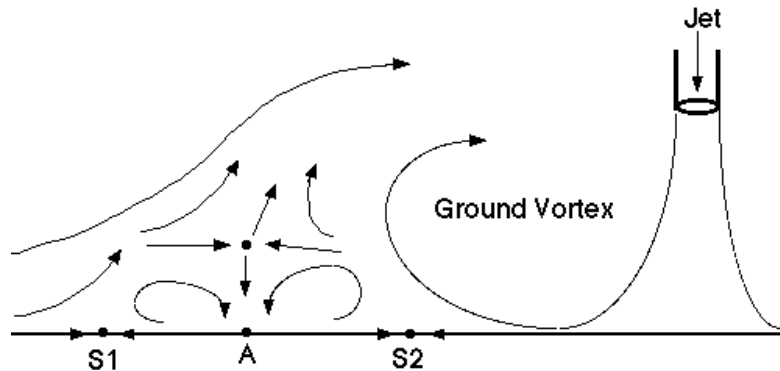

Fig. 7   Typical oil flow on the ground plane and in a cutting plane through the center of the domain.

computational equivalent of the smokewire. Particles are released from a vertical rake in the center plane ahead of the vortex. The streak lines are then computed to assess the behavior of the vortex. In their experiments, Cimbala et al. describe a behavior of the flow field which can be seen in a movie made from the present streakline calculations. Frames of the movie at regular time interval are presented in Figs. 8. These figures show a single puffing cycle to illustrate the unsteady behavior. Figures 8a and 8b show a vortex in development and getting larger. Figure 8c shows a vortex that is bending forward in order to sustain its size. Figure 8d shows mass being ejected by the vortex. Figure 8e shows the mass being washed down stream and Figs. 8f-g show the redevelopment of the vortex. The frequency of the puffing is approximately 2Hz which compares well to the value reported by Cimbala et al. for these conditions.

American Institute of Aeronautics and Astronautics

The behavior of the flow field is extremely unsteady and three dimensional. The location, size, and shape of the vortex changes continuously as noted by Cimbala et al. However, the basic unsteadiness can be described as a low frequency puffing of the ground vortex. The unsteadiness of the vortex matches that described by Cimbala et al. including the cycle of vortex growth, violent break up and the growth of a new vortex in its place.

In addition, a highly three dimensional flow field is seen in our simulations where the effect of a puffing of the vortex is propagated from the center of the vortex down stream and so the puffing it self seems to propagate through the vortex rather than the entire vortex puffing at the same time.

Physical Model

In order to simulate a complex flow field, with interactions such as a jet impinging upon a ground plane, and a three-dimensional, unsteady, boundary layer separation, an appropriate turbulence model must be carefully chosen and applied. The current work concentrates on the turbulence modeling requirement to simulate the unsteady ground vortex puffing described in the previous sections. Fig. 9 shows eddy viscosity contours through the lateral symmetry plane for a fully-developed turbulent simulation using the standard Spalart-Allmaras turbulence model[18]. A plot of eddy viscosity through the boundary layer and ground vortex core along the line shown in Fig. 9 is shown in Fig. 11. The eddy viscosity within the ground vortex is very large – approaching an order of magnitude larger than the eddy viscosity in the wall-bounded regions. Such a large turbulent eddy viscosity outside the boundary layer is not physically plausible, and leads to spurious results. In the current simulation, the large eddy viscosity effectively "damps out" the unsteadiness of the ground vortex puffing, and a steady (non-physical) solution is obtained.

The cause of the large eddy viscosity values in the vortex region is the production term in the turbulence model. This is similar to the difficulties encountered in applying standard turbulence models at high angles of attack, which also leads to strong vortices outside the boundary layer. The standard two-equation and algebraic models
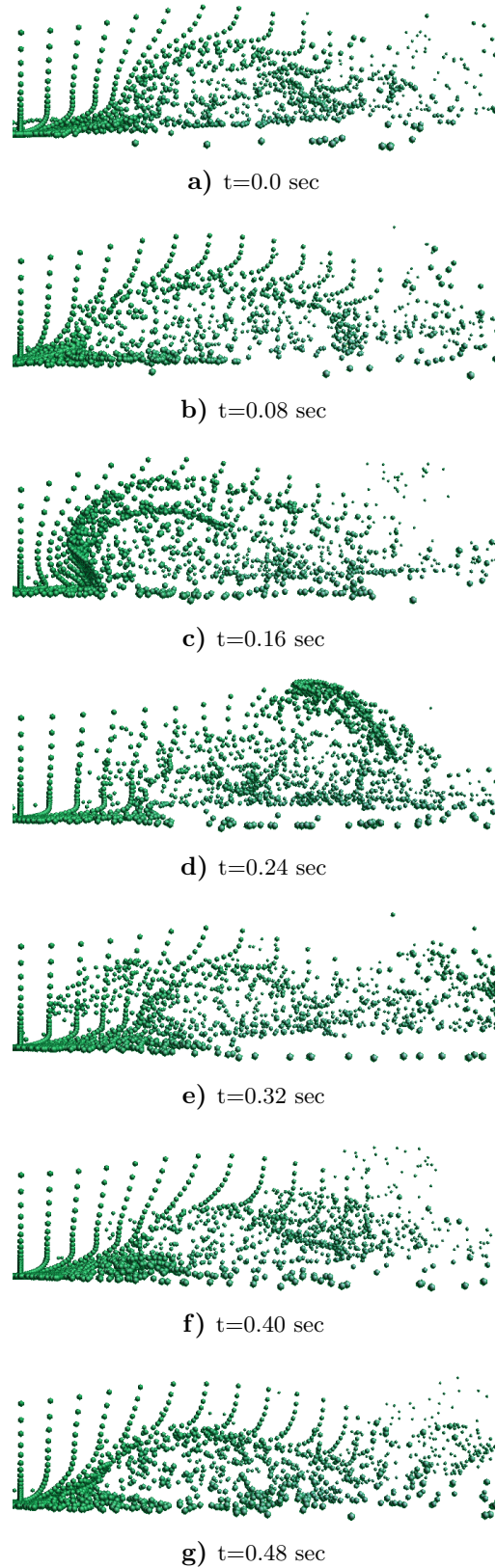

a) t=0.0 sec

b) t=0.08 sec

c) t=0.16 sec

d) t=0.24 sec

e) t=0.32 sec

f) t=0.40 sec

g) t=0.48 sec

Fig. 8   Smokewire time history: Snapshots of Streak lines computed from a vertical rake for the case of $M_\infty = 0.013$ and $M_{jet} = 0.13$.
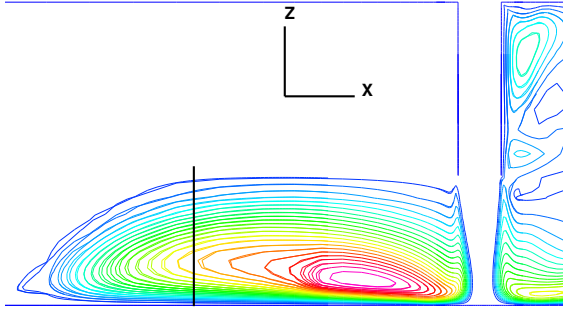
American Institute of Aeronautics and Astronautics

Fig. 9   Eddy viscosity in the vortex region for the Spalart-Allmaras turbulence model. The solid vertical line corresponds to Fig. 11.
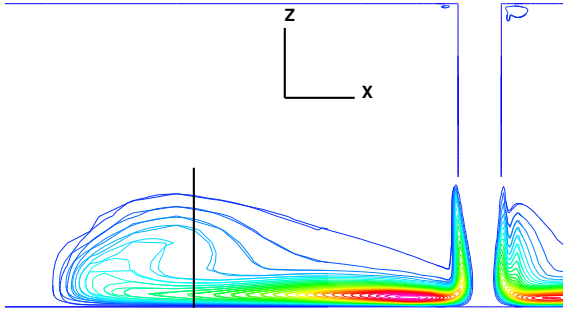

Fig. 10   Eddy viscosity in the vortex region for the Spalart-Allmaras turbulence model with a production cutoff. The solid vertical line corresponds to Fig. 11.

Fig. 11   Eddy viscosity in the vortex region for the Spalart-Allmaras turbulence model with a production cutoff.

also produce spurious eddy viscosity in such situations, and the production terms in the standard models must be modified in some manner[19]. One severe approach is to treat the ground vortex as an inviscid phenomena, and remove entirely the viscous terms and turbulence model entirely from this region. This leads to an unsteady flow field, however the flow in very chaotic, and no coherent structures form. The approach taken in the current work is to limit the production of eddy viscosity outside the boundary layer regions, following Murman[19]. The eddy viscosity contours for this production limit are shown in Fig. 10. The values along the vertical bar are plotted in Fig. 11. The eddy viscosity generated in the jet impingement and boundary layer regions is convected into the ground vortex, and then the turbulence in the vortex begins to dissipate without any source of production. This production-limited S-A model is used in all calculations presented here, and leads to the unsteady vortex puffing shown in Fig. 8.
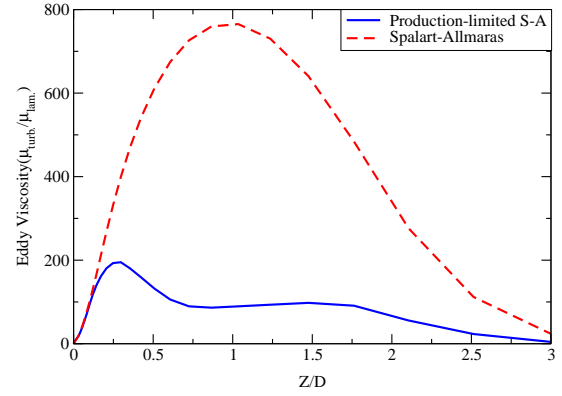
Wall Effects

In order to ascertain what effect the presence of wind tunnel walls has on the flow characteristics, a simulation is conducted without the wall. The resulting solution exhibits the same unsteady character with negligible change in the the ground vortex puffing behavior. However, the flow field does not have as much three dimensional variation. The vortex is always more coherent and the puffing of the vortex is a symmetric phenomenon occurring on both sides of the jet in unison. Figure 12 shows an overview of the flow field without the walls. Once again, the von Kármán vortex street is seen behind the jet tube and the horseshoe shaped ground vortex is present ahead of the jet.

Variation of Crossflow Velocity

The representative solution demonstrated that the correct flow physics can be obtained with appropriate computational methods (e.g. low-Mach number preconditioner) and proper modeling of turbulence. To verify that the method is useful over a range of conditions, the crossflow velocity is varied and the vortex center height and separation location are compared to the experimental results of Ref. [3]. Figure 13 shows the vortex center height as a function of V_∞. The computational results compare well with the experimental data. This verifies that as the crossflow velocity increases, the vortex becomes smaller in height.

The separation distance for the separation point S_2 along the cutting plane in the center is shown in Fig. 14 as a function of the crossflow velocity. The numerical simulations predict the
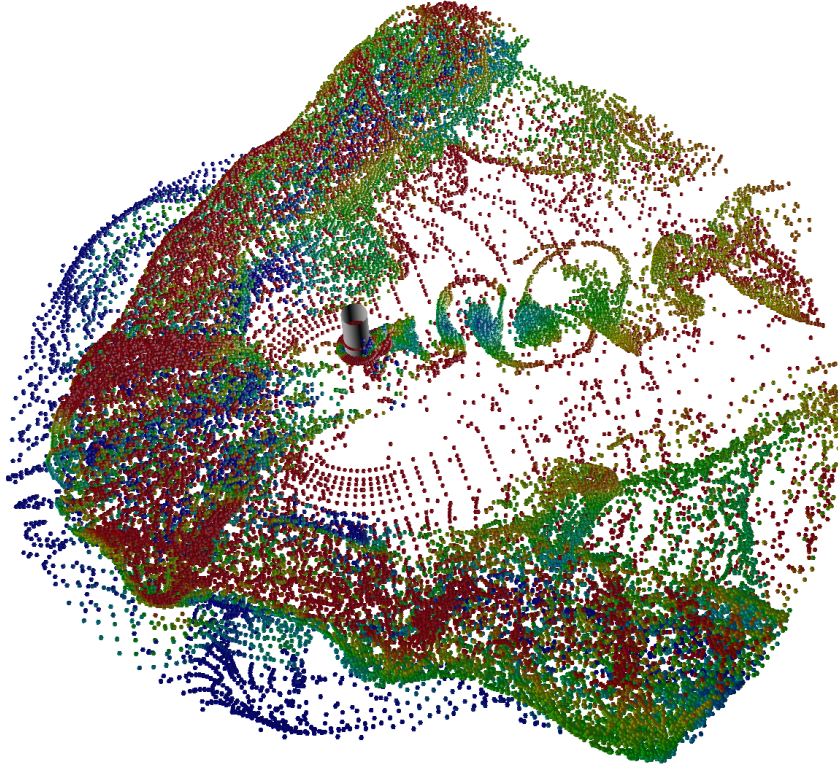
American Institute of Aeronautics and Astronautics

Fig. 12   Overview of the flow field for $M_\infty = 0.013$, $M_{jet} = 0.13$ without wind tunnel walls.
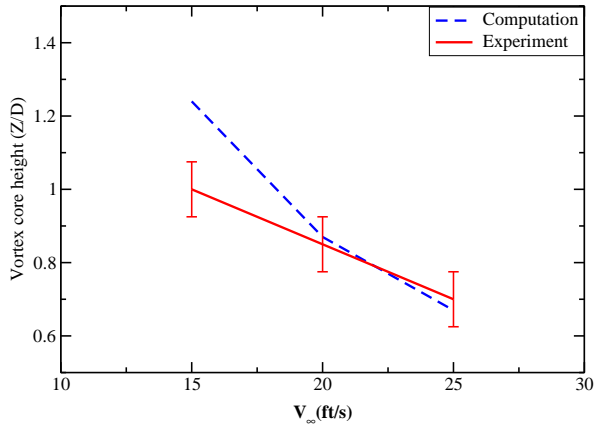

Fig. 13   Height of the center of the ground vortex as a function of V_∞. Comparison to Cimbala et al.[3].
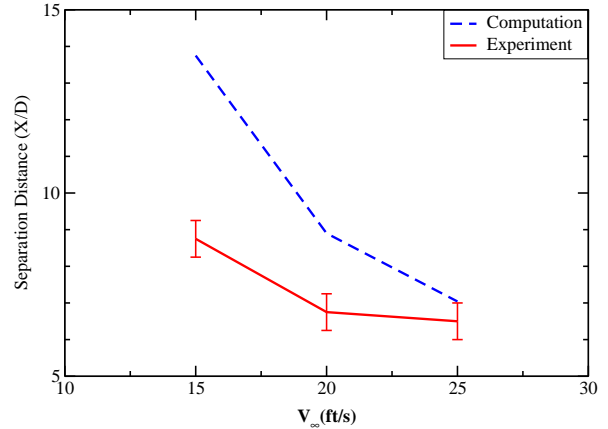

Fig. 14   Separation location as a function of V_∞. Comparison to Cimbala et al.[3].

same trends as the experiment; the ground vortex separation location moves farther from the jet impingement as the oncoming crossflow velocity decreases. Note that the oncoming flow separation (S1 in Fig. 7) was not mentioned by Cimbala et al.

Concluding Remarks

The flow of a single round jet impinging on a ground in low-speed crossflow is simulated using the dual-time preconditioned method in OVER-FLOW. Due to the robustness, efficiency and accuracy of this algorithm, it is possible to compute highly complex flow fields using a time step that is commensurate with the unsteady flow behavior

of interest. This leads to an order of magnitude improvement in CPU time required over a non-preconditioned system.

The results of the current simulation are compared to an experiment by Cimbala et al.[3]. These results show that with proper turbulence modeling and preconditioning, the gross features of the flow field (e.g. the jet impingement, puffing of the ground vortex, and von Kármán vortex street) are recovered. Furthermore, the unsteady behavior of the ground vortex is similar to that of the Cimbala et al. experiment. The size of the ground vortex is verified and the unsteady frequency matches that of Cimbala et al.'s experiment.

Acknowledgment

References

[1] P. E. Colin and D. Olivari. "The Impingement of a Circular Jet Normal to a Flat Surface with and without a Cross Flow". Final Technical Report TR-AD688953, von Kármán Institute, Jan. 1969. United States Defense Technical Information Center.

[2] J. M. Cimbala, D. R. Steinberg, A. L. Treaster, M. L. Billet, and M. M. Walters. "Experimental Investigation of a jet Impinging on a Ground Plane in Crossflow". *J. Aircraft*, 25(10):923–931, October 1988.

[3] J. M. Cimbala, M. L. Billet, D. P. Gaublomme, and J. C Oefelein. "Experiments on the Unsteadiness Associated with a Ground Vortex". *J. of Aircraft*, 28(4):261–267, April 1991.

[4] Jorge M. M. Barata. "Jets in Ground Effect with a Crossflow". AIAA Paper 97-0715.

[5] W. R. Van Dalsem. "Study of Jet in Ground Effect with Crossflow Using the Fortified Navier-Stokes Scheme". AIAA Paper No. 87-2279.

[6] M. H. Smith, K. Chawla, and W. R. Van Dalsem. "Numerical Simulation of a Complete STOVL Aircraft in Ground Effect". AIAA Paper No. 91-3293.

[7] Jorge M. M. Barata and D. F. G. Durao. "Numerical Study of Single Impinging Jets Through a Crossflow". *J. Aircraft*, 26(11):1002–1008, November 1989.

[8] Jorge M. M. Barata, D. F. G. Durao, and M. V. Heitor. "Impingement of Single and Twin Turbulent Jets Through a Crossflow". *AIAA Journal*, 29(4):595–602, April 1991.

[9] N. M. Chaderjian, S. Pandya, J. Ahmad, and S. M. Murman. "Parametric Time-Dependent Navier-Stokes Computations for a YAV-8B Harrier in Ground Effect". AIAA Paper No. 2002-0950.

[10] S. A. Pandya, N. Chaderjian, and J. Ahmad. "Parametric Study of a YAV-8B Harrier in Ground Effect Using Time-Dependent Navier-Stokes Computations". AIAA Paper No. 2002-3056.

[11] P. G. Buning, D. C. Jespersen, T. H. Pulliam, W. M. Chan, J. P. Slotnick, S. E. Krist, and K. J. Renze. "OVERFLOW User's manual". NASA.

[12] S. A. Pandya, S. Venkateswaran, and T. Pulliam. "Implementation of Preconditioned Dual-Time Procedures in OVERFLOW". AIAA Paper No. 2003-0072.

[13] S. Venkateswaran and C. L. Merkle. "Dual time stepping and preconditioning for unsteady computations". AIAA Paper No. 95-0078.

[14] P. E. O. Buelow, D. A. Schwer, J. Feng, and C. L. Merkel. "A preconditioned Dual-Time, Diagonalized ADI Scheme for Unsteady Computations". AIAA Paper No. 97-2101.

[15] T. H. Pulliam and D. S. Chausee. "A diagonal form of an implicit approximate-factorization algorithm". *Journal of Computational Physics*, 39(2):347–363, 1981.

[16] J. L. Steger, F. C. Dougherty, and J. A. Benek. "A Chimera Grid Scheme". In K. N. Ghia and U. Ghia, editors, *Advances in Grid Generation*, volume 5 of *ASME FED*. June 1983.

[17] J. A. Benek, P. G. Buning, and J. L. Steger. "A 3-D Chimera Grid Embedding Technique". AIAA Paper 85–1523, July 1985.

[18] P. R. Spalart and S. R. Allmaras. "A One-Equation Turbulence Model for Aerodynamic Flows". AIAA Paper 92-0439, January 1992.

[19] S. M. Murman. "Vortex Filtering for Turbulence Models Applied to Crossflow Separation". AIAA Paper 2001-0114, Jan. 2001.